Available online at www.sciencedirect.com

ScienceDirect

Ceramics International 40 (2014) 4231–4235

CERAMICS INTERNATIONAL

www.elsevier.com/locate/ceramint

Compressive creep behavior of spark plasma sintered La_2O_3–YSZ composite

K.D. Robles Arellano[a], L. Bichler[a,*], K. Mondal[a,b]

[a]School of Engineering, University of British Columbia – Okanagan, 3333 University Way, Kelowna, Canada V1V 1V7
[b]Department of Materials Science and Engineering, Indian Institute of Technology, Kanpur 208016, India

Received 8 July 2013; received in revised form 20 August 2013; accepted 20 August 2013
Available online 29 August 2013

Abstract

The present paper describes compressive creep behavior of cubic 8 mol% yttria stabilized zirconia + 10 mol% La_2O_3 (fabricated by Spark Plasma Sintering) in the temperature range of 1300–1330 °C at a stress level of 45–78 MPa in vacuum. The pre- and post-creep microstructures, relative magnitudes of the stress exponent ($n = 1.7$–2.1) and the activation energy (540–580 kJ/mol) suggest that grain boundary sliding aided by inter-diffusion of La and Zr leading to the formation of pyrochlore $La_{1.6}Y_{0.4}Zr_2O_7$ phase at the grain boundaries during creep is the active creep mechanism in this composite.
© 2013 Elsevier Ltd and Techna Group S.r.l. All rights reserved.

Keywords: A. Sintering; B. Composite; C. Creep; D. ZrO_2; La_2O_3

1. Introduction

Zirconia (ZrO_2) and its composites are attractive ceramic materials for engineering applications such as fuel cells, thermal barrier coatings and nuclear reactors, which demand high temperature stability, chemical inertness, low thermal conductivity and high fracture toughness [1–5]. However, suitable doping of ZrO_2 with divalent, trivalent or tetravalent ions such as Ca^{2+}, Mg^{2+}, Al^{3+}, Y^{3+}, and Ce^{4+} is necessary to stabilize the desirable tetragonal or cubic phases of zirconia at room temperature. Literature [6,7] suggests that addition of lanthanum dioxide (La_2O_3) to yttria stabilized zirconia (YSZ) up to 56 wt% may further improve the thermal insulating and hydrothermal degradation properties of the composite. However, most available literature [6–9] on the fabrication of the La_2O_3–YSZ composite is limited to conventional sintering (CS). Recent studies [10,11] indicate that high density (up to 99%) zirconia-based composites can be prepared via Spark Plasma Sintering (SPS) at lower sintering temperatures than those required by CS [8,9]. In addition, reports on the high temperature slow strain-rate creep behavior of CSed cubic zirconia suggest that the stress exponent (n) varies between 1 and 3, and the activation energy (Q) ranges between 480 and 600 $kJmol^{-1}$ depending on the grain size and test temperature [4,12]. In general, creep deformation associated with such values of n and Q suggests cation diffusion and grain boundary sliding. Recent study on SPS fabrication of cubic 8 mol % YSZ composites by the present authors has shown that high density fully stabilized cubic YSZ composites can be produced with the addition of up to 15 mol% La_2O_3 [13]. In this paper, the compressive creep behavior of the SPSed 10 mol% La_2O_3 + 8 mol% YSZ and its mechanism is studied through microstructural characterization and experimental measurement of n and Q values.

2. Materials and methods

A detailed procedure on the fabrication of the 10 mol% La_2O_3 + 8 mol% YSZ composite via SPS has been reported by the authors earlier [13]. Compressive creep testing on this composite was carried out at the Department of Physics of Condensed Matter at the University of Sevilla (Sevilla, Spain), using an uniaxial compressive creep frame equipped with an environmental (i.e., temperature and pressure controlled) chamber. Test specimens were cut from the center portion of the as-sintered discs and were sectioned into parallelepipeds

*Corresponding author. Tel.: +1 250 807 8816; fax: +1 250 807 9850.
E-mail address: lukas.bichler@ubc.ca (L. Bichler).

0272-8842/$ - see front matter © 2013 Elsevier Ltd and Techna Group S.r.l. All rights reserved.
http://dx.doi.org/10.1016/j.ceramint.2013.08.086

($2.5 \times 2.5 \times 5\ mm^3$) with a diamond blade saw and a Struers® rectifier. The samples were mounted to SiC pistons attached to a load-frame using adhesive and then precision-aligned with the loading axis. Then, low vacuum ($\sim 10^{-3}$ mbar) was established in the chamber, followed by a temperature increase to 500 °C at 10 °C/min. Argon flushing was carried out and high vacuum ($\sim 10^{-7}$ mbar) was established. To enable calculation of n and Q, two sets of experimental measurements were carried out consecutively:

I. Constant temperature and variable stress measurement, followed by
II. constant stress and variable temperature measurement.

The general expression for creep at high temperatures is defined as [12]

$$\dot{\varepsilon} = A\sigma^n e^{-(Q/kT)} \quad (1)$$

where, A=atomic structure constant; σ=applied stress; n=stress exponent; Q=activation energy; k=Boltzmann's constant; $\dot{\varepsilon}$=strain rate and T=temperature. From Eq. 1, n and Q values can be obtained by performing the above two experiments and using the following expressions [12]:

$$\frac{\dot{\varepsilon}_1}{\dot{\varepsilon}_2} = \frac{\sigma_1^n}{\sigma_2^n} \quad (2)$$

$$Q = -R\left(\frac{\ln(\dot{\varepsilon}_2 - \ln(\dot{\varepsilon}_1)}{1/T_2 - 1/T_1}\right) \quad (3)$$

Where R=gas constant. The compressive stress levels investigated in this research ranged between 45–78 MPa for the temperature range of 1300–1330 °C. The experiment was initiated at a stress magnitude of 76.8 MPa, followed by a stress decrease to 60.6 MPa and 45.1 MPa, concluding with a stress increase to 60 MPa, while the temperature was maintained at 1300 °C. Subsequently, the stress value remained constant and the ambient temperature was raised to 1330 °C, followed by a stress increase to 78 MPa at 1330 °C. This experimental sequence has been intentionally followed to study the effect of the applied stress on the creep strain rate at constant temperature, and also to study the effect of temperature on the strain rate.

A Tescan MIRA3 XMU scanning electron microscope with Oxford X-max EDS detector were used for microstructural observation and chemical analysis before and after creep. X-ray diffraction (XRD) of the composites was carried out with the X'Pert Pro (PANalytical) X-ray diffractometer with Bragg–Brentano set-up, equipped with X'Celeratrim in a 2θ range of 20–90° using 0.02° step size and 20 s time per step. Cu-K_α radiation with λ=0.1541 nm was used.

3. Results and discussion

3.1. Compressive creep

Fig. 1 shows the experimentally obtained $\dot{\varepsilon}$ vs. ε plot. This plot is a summary of all experiments (in the order as experiments have been performed as outlined in the preceding section) corresponding to the various stress and temperature ranges up to the final compressive strain of ~13.5%. It is observed that as the initial stress of 76.8 MPa is applied (or at any subsequent stress increase), a time dependent $\dot{\varepsilon}$ decrease is observed (initial curvature) until a stable plateau is achieved. In contrast, a lowering in the magnitude of the applied stress at a constant temperature results in a reversal of the curved portion in the $\dot{\varepsilon}$ vs. ε plot, as seen during a subsequent test where the applied stress is lowered to 60.6 MPa. These time-dependent phenomena are related to the gradual transition between the onset of plastic deformation and stage II creep at the beginning of each creep test segment. Also, Fig. 1 shows that the magnitude of the plateau of $\dot{\varepsilon}$ varies with the level of applied stress at a constant temperature, and similarly the magnitude of the plateau of $\dot{\varepsilon}$ varies as a function of temperature at constant applied stress. In the first case, the magnitude of the strain-rate plateau is governed by the applied stress, as expected. In the second case, the change of the plateau magnitude of the strain rate due to the increase in the temperature is related to the enhancement of the operative creep mechanism, which can be either grain boundary sliding, diffusion or mixed mode. The values of n range between 1.7 and 2.1 (as calculated from Eq. (2)), with specific values included in Fig. 1 above the vertical lines separating the discrete stress segments. The values of Q (as calculated from Eq. (3)) associated with each temperature regime vary between 546 and 586 kJ/mol.

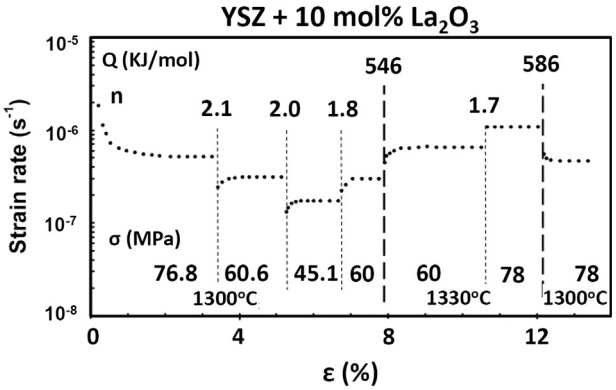

Fig. 1. Strain rate (QUOTE) vs. ε plots for the composite with the variation of stress and temperature. Values of n and Q are indicated above vertical lines in the figure.

3.2. Phase evolution

Fig. 2 shows XRD plots of the La_2O_3–YSZ composite before and after creep. Evident increase in the magnitude of the relative peaks corresponding to the pyrochlore lanthanate phase $La_{1.6}Y_{0.4}Zr_2O_7$ is observed. The fraction of pyrochlore phase in the before and after creep samples has been calculated by comparing the intensities of most intense peaks of the cubic YSZ (at 2θ=30.03°) and the pyrochlore phase (2θ=28.79°). The results suggest that the pyrochlore amount increases from 4.3 wt% in the as-sintered composite to 14.5 wt% in the after creep composite. The mechanism of formation of this phase

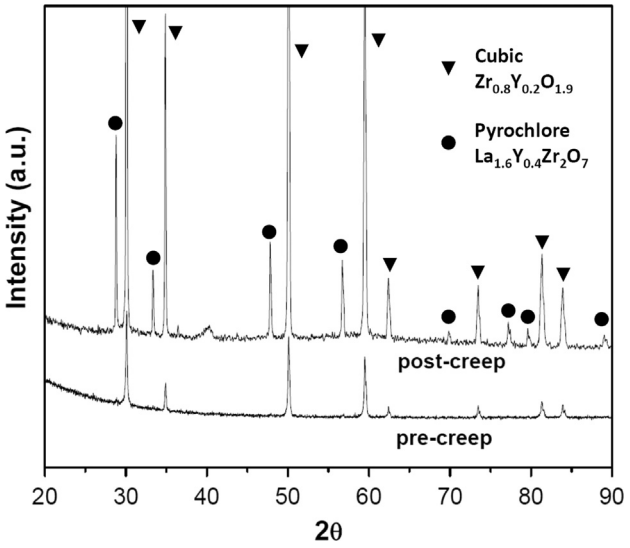

Fig. 2. XRD patterns of the La_2O_3–YSZ composite before and after creep cycle.

Table 1
Composition of different regions of the composite before and after creep.

Region of interest	Zr	Y	La	O	Cl	Hf
YSZ matrix (pre-creep)	56	8.8	6	19	< 0.1	1.3
YSZ matrix (post-creep)	57	8.7	6.2	15	< 0.1	1.4
Lanthanate (pre-creep)	47	6.6	17	19	< 0.1	1
Lanthanate (post-creep)	45	5.7	23	15	< 0.1	1.2

during SPS processing has been described in our previous communication [13]. The enhanced formation of the pyrochlore lanthanate phase during creep is related to the progressive inter-diffusion of La and Zr along the grain boundaries, which is evident in Table 1 and the SEM – XEDS results. This is also discussed in the following section. Interestingly, despite the progressive cation inter-diffusion during creep, the structure of the YSZ matrix remains cubic.

3.3. Microstructure characterization

Fig. 3(a and b) shows representative micrographs of the La_2O_3–YSZ composite before and after creep, respectively. Both micrographs show a bi-modal grain structure. Composition analysis (Table 1) of the two grain families suggests that the large matrix grains are YSZ. The fine grains decorating the YSZ grains are highly enriched in La, Zr, Y and O. Thus, due to prolonged holding of the sample at high temperature during creep in conjunction with the applied action of stress, inter-diffusion of La and Zr has enabled the evolution of the fine grained La-rich phase with a stoichiometry consistent with the pyrochlore lanthanate phase ($La_{1.6}Y_{0.4}Zr_2O_7$), as confirmed by XRD analysis (Fig. 2). In the case of the post-creep sample, the pyrochlore phase is also seen to form within the YSZ matrix grains.

As indicated by arrows in Fig. 3(a and b), evolution of the pyrochlore lanthanate is associated with void formation at the grain boundary triple points, in both specimens before and after creep. Nucleation of the voids is likely to be associated with a localized volume expansion of the pyrochlore lanthanate-rich regions due to its higher molar volume than that of the cubic YSZ [14]. The local grain boundary separation might have originated from these voids, and subsequently has likely contributed to creep crack nucleation and further grain boundary separation, as observed in Fig. 3(c and d) near a crack tip.

Detailed examination of the pyrochlore lanthanate phase in Fig. 3(c), however, reveals that void formation is possibly not the primary mechanism of accommodating plastic deformation of the composite. Region 1 (indicated by a circle in Fig. 3(c)) clearly shows that on a large-scale crack propagation and growth readily occur once the pyrochlore lanthanate ligaments are torn. However, Region 2 in Fig. 3(c), enlarged in Fig. 3(d), confirms that the initial stage of creep is driven by grain boundary sliding. The onset of grain separation is manifested by the elongated necks in the pyrochlore lanthanate ligaments in regions where tensile strain evolved (marked as "T"), with concurrent sliding and shear deformation of the pyrochlore lanthanate ligaments in perpendicular direction (marked as "S") in Fig. 3(d). Although the pyrochlore lanthanate phase acts as a bridge between adjacent YSZ matrix grains, it has a lower yield strength and Young's modulus than that of the YSZ matrix grains [14]. Thus, the action of the applied stress and cation diffusion (as confirmed by present authors via X-ray line scans earlier [13]) along the grain boundary has likely weakened the grain boundary interface and allows for sliding. The arrows in Fig. 3(d) point to a diffuse interface boundary between the YSZ matrix and the pyrochlore lanthanate phase, suggesting that a time-dependent interdiffusion occurs at the grain boundaries during creep.

The stress exponent and activation energy for creep tests performed in the present study are within 1.7–2.1 and 530–580 kJ/mol, respectively. Literature [4,12,15] suggests that the stress exponent and activation energy for creep of YSZ are within the range observed in the present study if the creep mechanisms are associated with a mixed mode of cation diffusion assisted by grain boundary sliding (at test temperatures comparable to the present study). Therefore, the microstructural evidence in corroboration with the measured values of n and Q indicate that a mixed mode of grain boundary sliding and boundary diffusion are primary creep modes in the 10 mol% La_2O_3 + 8 mol% YSZ composite as well. The lack of published data on the activation energy for creep in La_2O_3–YSZ composites inhibits comparison of the measured Q values in this research to other studies.

4. Conclusions

The creep behavior of novel La_2O_3–YSZ composite prepared by Spark Plasma Sintering has been investigated. The results suggest that high temperature exposure of the composite during creep enables enhanced interdiffusion of La and Zr,

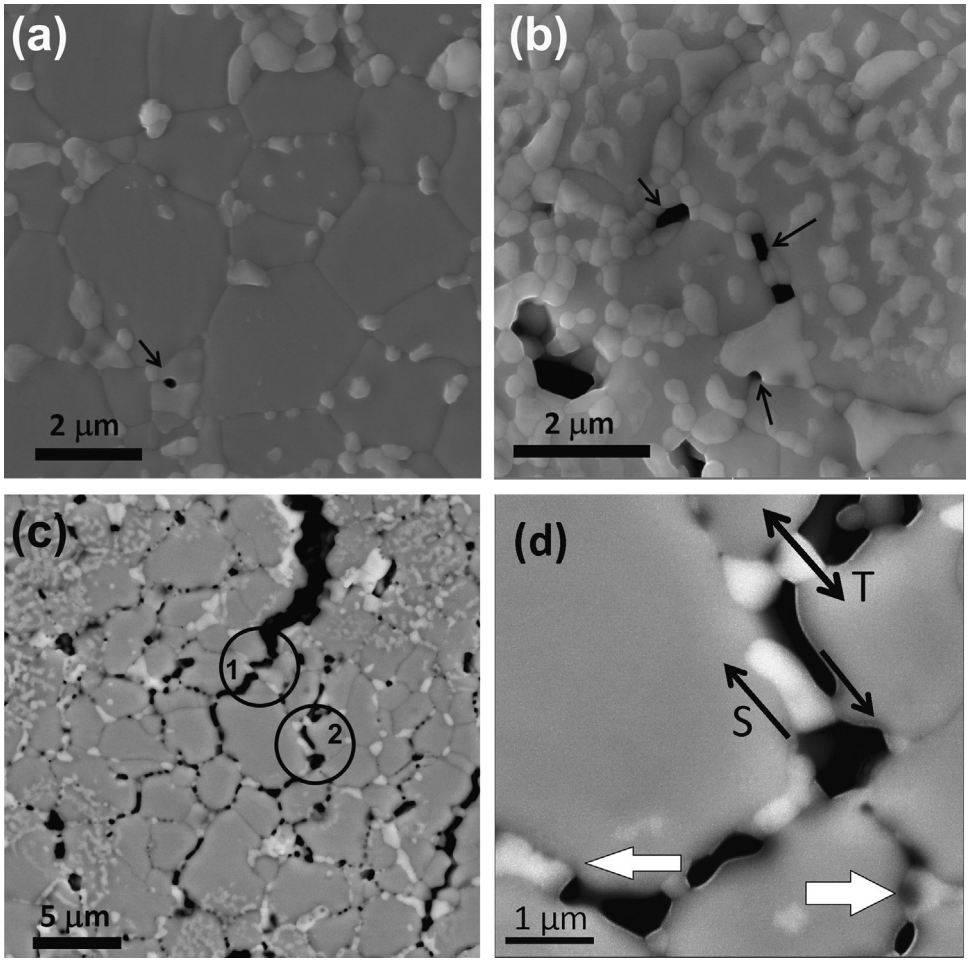

Fig. 3. Representative microstructure of sintered La_2O_3–YSZ composite: (a) before creep, (b) after creep, (c) creep induced intergranular cracking, and (d) detail of area "2" from Fig. 3c with regions of tensile (T) and shear (S) deformation.

resulting in the formation of pyrochlore lanthanate phase $La_{1.6}Y_{0.4}Zr_2O_7$ along the grain boundaries. The values of stress exponent and activation energy obtained in this work suggest that grain boundary sliding and lattice diffusion have been primary creep controlling mechanisms.

Acknowledgments

The authors wish to acknowledge Mr. M. van Hanegem, Ms. A. Siebert-Timmer and Mr. D. Arkinstall from the University of British Columbia, Prof. B. S. Murty, Mr. S. Ipe Varghese and Mr. K. Akkiraju from the Indian Institute of Technology Madras, and Dr. A. Dominguez-Rodriguez, Dr. M. Castillo Rodriguez and D. A. Munoz from Universidad de Sevilla. The financial support of the Natural Sciences and Engineering Research Council of Canada is gratefully acknowledged.

References

[1] O.A. Graeve, "Ch 10: Zirconia," in Ceramic and Glass Materials: Structure, in: J.F. Shackelford, R.H. Doremus (Eds.), Properties and Processing, Springer, Davis, CA, 2008, pp. 169–197.

[2] T. Xu, J. Vleugels, O. Van der Biest, P. Wang, Mechanical properties of Nd_2O_3–Y_2O_3-coated zirconia ceramics, Materials Science and Engineering 374 (2004) 239.

[3] Z. Xu, L. He, X. Zhong, R. Mu, S. He, X. Cao, Thermal barrier coating of lanthanum–zirconium–cerium composite oxide made by electron beam-physical vapor deposition, Journal of Alloys and Compounds 478 (2009) 168.

[4] J. Wolfenstine, P. Huang, A. Petric, Creep behavior of doped lanthanum gallate versus cubic zirconia, Solid State Ionics 118 (1999) 257.

[5] J.A. Allemann, B. Michel, H.-B. Märki, L.J. Gauckler, E.M. Moser, Grain growth of differently doped zirconia, Journal of the European Ceramic Society 15 (1995) 951.

[6] S.A. Tsipas, Effect of dopants on the phase stability of zirconia-based plasma sprayed thermal barrier coatings, Journal of the European Ceramic Society 30 (2010) 61.

[7] B. Bastide, P. Odier, J.P. Coutures, Phase equilibrium and martensitic transformation in lanthana-doped zirconia, Journal of the American Ceramic Society 71 (6) (1988) 449.

[8] P. Singh, S.R. Sainkar, M.V. Kuber, V.G. Gunjikar, R.F. Shinde, S. K. Date, La-stabilized zirconia: synthesis and characterization, Materials Letters 9 (1990) 65.

[9] C. Wang, Y. Wang, Y. Cheng, W. Huang, Z.S. Khan, X. Fan, Y. Wang, B. Zou, X. Cao, Preparation and thermophysical properties of nano-sized $Ln_2Zr_2O_7$ (Ln=La, Nd, Sm, and Gd) ceramics with pyrochlore structure, Journal of Materials Science 47 (2012) 4392.

[10] Y. Bangchao, J. Jiawen, Z. Yican, Spark-plasma sintering the 8 mol% yttria-stabilized zirconia electrolyte, Journal of Materials Science 39 (2004) 6863.

[11] K. Khor, L.G. Yu, S. Chan, X. Chen, Densification of plasma sprayed YSZ electrolytes by spark plasma sintering (SPS), Journal of the European Ceramic Society 23 (2003) 1855.

[12] M. Jimenez-Melendo, A. Dominguez-Rodriguez, A. Bravo-Leon, Superplastic flow of fine-grained yttria-stabilized zirconia polycrystals: constitutive equation and deformation mechanisms, Journal of the American Ceramic Society 76 (1998) 2761.

[13] K.D. Robles Arellano, L. Bichler, K. Akkiraju, R. Fong, K. Mondal, Densification behavior of spark plasma sintered La_2O_3–YSZ ceramic composites, Ceramics International (2013), http://dx.doi.org/10.1016/j.ceramint.2013.06.060 (in press).

[14] B. Liu, J.Y. Wang, J.C. Zhou, T. Liao, F.Z. Li, B. Liu, Theoretical elastic stiffness, structure stability and thermal conductivity of $La_2Zr_2O_7$ pyrochlore, Acta Materialia 55 (2007) 2949.

[15] R.G. St-Jaques, R. Angers, CaO-stabilized ZrO_2, Journal of the American Ceramic Society 55 (1972) 571.